Check for updates

Raman Spectroscopy Hot Paper

How to cite: *Angew. Chem. Int. Ed.* **2021**, *60*, 22004 – 22009
International Edition: doi.org/10.1002/anie.202109345
German Edition: doi.org/10.1002/ange.202109345

Can One Measure Resonance Raman Optical Activity?

Guojie Li, Mutasem Alshalalfeh, Yanqing Yang, James R. Cheeseman, Petr Bouř, and Yunjie Xu**

Abstract: *Resonance Raman optical activity (RROA) is commonly measured as the difference in intensity of Raman scattered right and left circularly polarized light, $I_R - I_L$, when a randomly polarized light is in resonance with a chiral molecule. Strong and sometimes mono-signate experimental RROA spectra of several chiral solutes were reported previously, although their signs and relative intensities could not be reproduced theoretically. By examining multiple light-matter interaction events which can occur simultaneously under resonance, we show that a new form of chiral Raman spectroscopy, eCP-Raman, a combination of electronic circular dichroism and circularly polarized Raman, prevails. By incorporating the finite-lifetime approach for resonance, the experimental patterns of the model chiral solutes are captured theoretically by eCP-Raman, without any RROA contribution. The results open opportunity for applications of eCP-Raman spectroscopy and for extracting true RROA experimentally.*

Introduction

Raman spectroscopy is a powerful spectroscopic tool for elucidating structural information. The chiral version of Raman spectroscopy, Raman optical activity (ROA),[1] has been utilized substantially to characterize absolute configurations and conformational distribution dynamics of many biomolecules[2] and (in)organic molecules.[3] A known experimental limitation is the weakness of the Raman signal. This is even more severe for ROA intensity of which is typically only 10^{-3}–10^{-4} of that of Raman.[1b] Researchers have been therefore exploring the resonance regime when the excitation laser frequency is in (near) resonance with one or multiple electronic transitions of a chiral molecule to enhance its ROA intensity. Such resonance ROA (RROA) enhancements have been reported for naproxen and its derivatives,[4] transition metal complexes,[5] carotenoid aggregation,[6] and biological systems.[7] Also following the advances of surface enhanced Raman spectroscopy (SERS) development, some exciting works on surface enhanced ROA (SEROA) have appeared.[8] The combination of these two methods, that is, surface enhanced RROA (SERROA), has also been reported, for example, for myoglobin.[9]

Another significant challenge is how to interpret the observed chiral Raman spectra under resonance conditions. These spectral patterns often do not show any resemblance to the corresponding far-off resonance spectra that can be predicted pretty reliably with DFT calculations.[10] In the case when only a single electronic state (SES) is in resonance with the excitation laser wavelength, the SES theory pioneered by Nafie predicts that the ratio of RROA to resonance Raman (RRaman) in the most common SCP experiment equals to −1/2 times the ratio of electronic circular dichroism (ECD) to absorption.[11] As a result, the mono-signate ROA feature is often regarded as a hallmark of RROA and has been utilized to interpret experimental ROA results in many subsequent publications when (near) resonance is present.[5,7] For example, S. Haraguchi et al.[7] reported an RROA spectrum of a photoreceptor protein in resonance with the laser excitation at 532 nm and showing a mono-sign, opposite to that of the singlet resonant state, as anticipated. Very recently, a mono-signate RROA was reported for a chiral naphthalenediimide derivative (abbreviated as **BN** in Figure 1).[12] A perplexing observation was that the experimental RROA sign of **BN** is the same as the ECD of the corresponding (near) resonance electronic transition, contrary to the SES prediction. To explain this observation, the authors proposed two **BN** conformers with (near) resonance electronic transitions

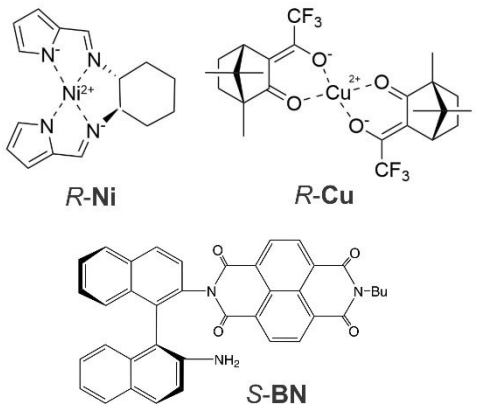

Figure 1. The three chiral compounds discussed: (*R*,*R*)-bis (pyrrol-2-ylmethyleneamine)-cyclohexane nickel^{II} (*R*-**Ni**), *R*-bis-(trifluoroacetyl camphorato) copper^{II} (*R*-**Cu**), and atropisomeric naphthalenediimide derivative, *S*-nBu-NDI-BINAM (*S*-**BN**), which consists of binaphthalenylamine (BINAM) and naphthalene (NDI).

[*] G. Li, M. Alshalalfeh, Y. Yang, Prof. Dr. Y. Xu
Department of Chemistry, University of Alberta
Edmonton, Alberta, T6G 2G2 (Canada)
E-mail: yunjie.xu@ualberta.ca
Dr. J. R. Cheeseman
Gaussian Inc.
340 Quinnipiac St., Bldg. 40, Wallingford, CT 06492-4050 (USA)
Prof. Dr. P. Bouř
Institute of Organic Chemistry and Biochemistry
Flemingovo náměstí 2, 16610, Prague (Czech Republic)
E-mail: bour@uochb.cas.cz
Supporting information and the ORCID identification number(s) for the author(s) of this article can be found under: https://doi.org/10.1002/anie.202109345.

 © 2021 Wiley-VCH GmbH

having opposite ECD signs, and that one conformer dominates the ground and the other the excited state. The SES theory was then invoked to explain the surprising RROA sign-switching based on the conformer in the excited electronic state.

More recent theoretical developments show that by considering excited state interference and Herzberg–Teller effects, a multi-signate RROA showing intensity enhancement in RROA spectra can be produced.[13] Other approaches to treat RROA, such as using time-dependent (TD) formulation and real time propagation TDDFT, have also been developed.[14] DFT calculations have been compared to the experimental RROA of medium-size organic molecules such as naproxen sodium, quinidine and 2-Br-hexahelicen, as well as some transition metal complexes.[14c,15]

When a chiral molecule is under (near) resonance in an ROA experiment, several light-matter interaction events can occur at the same time. These include absorption, ECD, and Rayleigh and Raman scattering as well as their polarized forms. These complications have not been addressed before or have been commonly ignored in the RROA research literature. Herein, we show that a new form of resonance Raman spectroscopy of natural chirality can be carried out using a ROA instrument under (near) resonance condition. This new spectroscopy can be regarded as a combination of ECD and circularly polarized-Raman[1] (CP-Raman). We abbreviate it as eCP-Raman, in a similar fashion that magneto-chiral dichroism (MChD) can be regarded as a product of ECD and magnetic CD.[16] Using three chiral compounds as examples, we demonstrate that in these cases, natural RROA is completely masked by this effect. The recently developed finite-lifetime approach for resonance (see Computational Details in the Supporting Information) provides good agreement with the experimental observations. Finally, we comment on the possibility of detecting the true RROA experimentally, which we find to be a crucial point in the development of current RROA methodology.

Results and Discussion

Strong induced solvent ROA patterns were observed in recent studies of chirality transfer from a chiral solute under resonance to a series of achiral solvents.[5,17,18] Several chirality induction mechanisms were proposed, such as solvent-chiral solute interactions, similar to those used to explain induced solvent vibrational circular dichroism features,[19] or an ad hoc "ring of fire" mechanism[17] where chiral Rayleigh scattering appears to contribute significantly. Some noticeable discrepancies between experiment and theory remained between these two proposals. Later on, it was recognized the induced solvent ROA patterns could be satisfactorily interpreted by ECD and polarized Raman scattering.[18]

In light of these findings, we focus on interpretation of experimental $I_R - I_L$ features of three chiral solutes (shown in Figure 1) under resonance, which were previously regarded as RROA. These are two transition metal complexes, *R*-**Ni**[20] and *R*-**Cu**,[5] and one organic molecule, *S*-**BN**.[12] These systems show both multi-signate and mono-signate $I_R - I_L$ patterns. Although some interpretations were presented before, based on the SES theory,[5,12] no theoretical simulations of the spectra were reported.

To detect a RROA spectrum, a chiral target needs to be in (near) resonance with the incident laser light, at 532 nm for the current study. One well-known experimental challenge is the interference of the fluorescence with the Raman scattering. In addition, UV/Vis absorption may be too strong, leaving little light for Raman scattering. It is generally assumed that good-quality mirror-image ROA spectra for a pair of chiral solute enantiomers are proof of true RROA. Unfortunately, such assumption oversimplifies the real situation. We noticed this first in the **Ni** system, where the metal centers provide extremely large magnetic dipole moments in the *d-d* electronic transitions. Therefore the ratio of ECD to UV/Vis absorption is high.[17] Consequently, even though by absorbance at 532 nm only a few percent of the light is lost, a strong ECD causes noticeable imbalance of the right versus left circularly polarized light (RCPL/LCPL). This imbalance in RCPL/LCPL then leads to CP-Raman scattering.[1] as previously reported by Clark et al. in 1974[21] and by others.[22] By recording $I_R - I_L$ using 100% LCPL for the excitation, these authors obtained a multi-signate CP-Raman of several common solvents such as chloroform.[21] The CP-Raman intensity and sign can be predicted using only components of the electric-dipole–electric-dipole polarizability tensor, as in the case of Raman.[1,22]

Nowadays, the majority of ROA measurements utilize the scattered circular polarized (SCP) backscattering setup,[23] where a randomly polarized light shines on a chiral sample and the $I_R - I_L$ signal is registered. Under resonance, the imbalance in $I_R - I_L$, produced by ECD of the chiral solute, leads to CP-Raman intensity, which is collected in the same spectrum as natural RROA. In addition, the out-going Raman scattering is again subjected to the ECD process. Therefore, an RROA signal thus measured is generally contaminated by eCP-Raman. In other words, the $I_R - I_L$ signal thus collected contains both RROA and eCP-Raman contributions. For eCP-Raman, Equation (1) was derived:[18]

$$CID = \frac{I_R - I_L}{I_R + I_L} = \frac{ln10}{4} cL\Delta\varepsilon \left(\frac{\Delta\varepsilon'}{\Delta\varepsilon} + DOC \right) \quad (1)$$

Here $\Delta\varepsilon$ and $\Delta\varepsilon'$ are differential absorption indices for the excitation and scattered light, that is at 532 nm ($\Delta\varepsilon$) and at each Raman band ($\Delta\varepsilon'$). c is the concentration of the chiral solute, L is the optical path length, and DOC is the degree of circularity[1] of each vibrational transition of either the solute or solvent. Please note that the DOC term here is used to calculate sign and intensity of CP-Raman (not ROA) bands and is defined for backscattering geometry when RCPL is applied.[1] I_R and I_L are the intensities of scattered RCPL and LCPL registered at the ROA instrument, respectively. We will use Equation (1) to evaluate eCP-Raman contributions of both achiral solvents and chiral solutes in the three examples considered.

 © 2021 Wiley-VCH GmbH

It is important to point out that simulations of I_R-I_L signals of achiral solvents generally do not involve any resonance calculations as they are transparent at 532 nm. Since achiral solvents do not have their own ROA intensity, the solvent I_R-I_L signals contain only eCP-Raman contributions and can be evaluated based on Equation (1). While the solvent *DOC* curves can be obtained by ratioing the solvent CP-Raman and Raman spectra calculated using the usual far-off resonance calculations, the chiral solute contributions, that is, $\Delta\varepsilon$ value at 532 nm and $\Delta\varepsilon'$ curve can be taken directly from the experimental measurements. Such evaluations were demonstrated in Ref. [18].

Simulating the I_R-I_L signal of a chiral solute under resonance, on the other hand, is more complicated, as it may contain variable contributions from both RROA and eCP-Raman. Furthermore, (near) resonance effects may be significant and need to be properly accounted for in the calculations of Raman, CP-Raman, and RROA. We applied the finite-lifetime (or damped response) approach, similar to that described previously[24] to treat the resonance effect in its Raman, CP-Raman and ROA spectra, using the Gaussian Development Version (GDV) package.[25] The simulation of CP-Raman requires only the same polarizability tensors (electric-dipole–electric-dipole, α) as for Raman and not the electric-dipole–magnetic-dipole and electric-dipole–electric-quadrupole polarizabilities (G' and A, respectively) as needed for ROA.[1] In the finite-lifetime approach, an imaginary phenomenological damping parameter, γ, is added to the incident frequency, ω, where γ is related to the lifetime of the excited states and to the widths of the absorption (or dispersion) peaks.[24] While previous implementations were numerical (i.e. numerically differentiating the α, G' and A polarizability tensors with respect to nuclear coordinates, generally requiring substantial computational time), the current fully analytic derivative implementation in the GDV additionally includes magnetic field dependent basis functions (GIAOs) which insure gauge origin-independent results and typically takes about 1.5 to 2 times longer than a normal Raman and ROA calculation (i.e. without the finite-lifetime approach) with G16.[26]

Geometry optimizations, harmonic frequency, Raman, CP-Raman and ROA calculations at 532 nm for *R*-**Ni** and *R*-**Cu** were performed using the GDV package.[25] eCP-Raman spectrum of *R*-**Ni** (or *R*-**Cu**) under (near) resonance was simulated by multiplying its simulated RRaman spectrum with CID from Equation (1). Experimental $\Delta\varepsilon$ at 532 nm and the $\Delta\varepsilon'$ curve in the range from 532 nm to 590 nm (corresponding to 0–1850 cm^{-1} on the Raman scale) were used, while the *DOC* was obtained from DFT. While it is possible to evaluate $\Delta\varepsilon$ and $\Delta\varepsilon'$ based on ab initio calculations as well, the accuracy of the current ECD calculations is not yet sufficient to yield reliable eCP-Raman predictions.

For the damping parameter, $\gamma = 880\ cm^{-1}$, as suggested by others,[24] was used. We also tested the sensitivity of simulated Raman, CP-Raman and RROA spectra of *R*-**Ni** to this damping parameter, by using $\gamma = 988\ cm^{-1}$, $880\ cm^{-1}$ and $550\ cm^{-1}$. The comparisons are summarized in the Supporting Information, Figure S1. The three values give more or less the same results for Raman and CP-Raman, which are directly relevant to the current eCP-Raman simulations, while some small differences appear for RROA in the lower cm^{-1} region.

For *R*-**Ni**, the optimized geometry and harmonic frequencies were computed at the B3LYP/aug-cc-pVTZ level of theory. We also tested the sensitivity of the simulated Raman, CP-Raman and RROA spectrum of *R*-**Ni** to different basis sets such as aug(sp)-cc-pVDZ and aug-cc-pVDZ. The results with the additional basis sets are provided in the Supporting Information, Figure S2. As can be seen in Figure S2, essentially identical spectra were predicted with all basis sets tried.

Other parameters used to simulate the eCP-Raman and RROA spectra are provided in Experimental Details and Computational Details in the Supporting Information. For example, the concentration of *R*-**Ni** was 0.037 M and the path length 0.25 cm for the evaluation of CID. Note that this concentration would be too low for a non-resonant ROA experiment. The path length corresponds to half of the cell length since the laser focal point was approximately at the center of the cell. The DOC curve was simulated by taking the ratio of the associated CP-Raman versus Raman spectra of *R*-**Ni** extracted from the DFT calculations with the finite-lifetime approach. Finally, the eCP-Raman spectrum of *R*-**Ni** was calculated as Raman × CID from Equation (1). An analogous procedure was used for eCP-Raman of *R*-**Cu**.

In Figure 2, simulated I_R+I_L (Raman) and I_R-I_L (eCP-Raman) spectra of *R*-**Ni** and *R*-**Cu** based on Equation (1) are compared with experimental spectra of *R*-**Ni** in CH_2Cl_2 (DCM) and $CHCl_3$ and of *R*-**Cu** in DCM and $CHCl_3$,

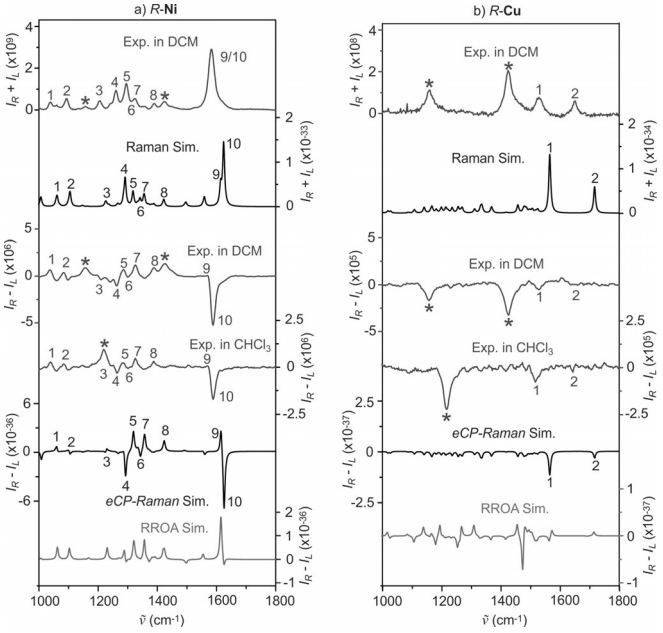

Figure 2. a) Top: experimental Raman (I_R+I_L) spectrum of *R*-**Ni** in CH_2Cl_2 is compared with the simulated solute *R*-**Ni** Raman; Bottom: experimental ROA (I_R-I_L) spectra of *R*-**Ni** in CH_2Cl_2 and in $CHCl_3$ are compared with simulated *R*-**Ni** eCP-Raman and with simulated natural RROA spectrum of *R*-**Ni**. b) Analogous results for *R*-**Cu**. Corresponding experimental and theoretical solute bands are numbered and asterisk (*) indicates the experimental solvent bands. The calculated spectral intensities are displayed in units of [m^2 cm/sr] where m is meter and sr is steradian.

 © 2021 Wiley-VCH GmbH

respectively. Calculated natural RROA spectra of both chiral solutes at 532 nm are also provided. Several important observations can be made about Figure 2. First, the I_R+I_L (Raman) experimental spectral patterns of both **Ni** and **Cu** are well reproduced by the simulations. Second, the I_R-I_L experimental spectral patterns of *R*-**Ni** are essentially the same in both solvents, and the same can be said for *R*-**Cu**. In other words, there are no explicit solute-solvent interactions or formations of specific solute-solvent complexes to be concerned about. Third, somewhat surprisingly, the simulated I_R-I_L spectra based on Equation (1) are in very good agreement with the experimental I_R-I_L spectra for both **Ni** and **Cu**. The positive experimental I_R-I_L **Ni** feature near 1570 cm^{-1} looks less prominent than that in the simulated bi-signate features. This can be attributed to slightly broader experimental bands where the symmetric and asymmetric C=N stretching modes overlap. Fourth, the simulated CID magnitude is in the order of 10^{-3} for **Ni** and 10^{-4} for **Cu**, in good agreement with the related experimental magnitudes, capturing the difference between **Ni** and **Cu**. Indeed, the experimental I_R-I_L signal of **Ni** emerged in a few minutes rather than 2–3 hours in the case of **Cu**. Fifth, the simulated natural RROA is drastically different from the experimental I_R-I_L spectral patterns for both **Ni** and **Cu**.

The simulated I_R+I_L (Raman) and I_R-I_L (eCP-Raman) spectra of both solvent and solute in the 250–2250 cm^{-1} region are depicted in the Supporting Information, Figure S3 for *R*-**Ni** and *R*-**Cu**, showing good agreement with the experimental data. Furthermore, the relative intensity of solvent to solute appears to be well reproduced for both I_R+I_L and I_R-I_L for *R*-**Cu**. For both I_R+I_L (Raman) and I_R-I_L (eCP-Raman) of *R*-**Ni**, the experimental *R*-**Ni** intensity relative to the respective solvent is ≈ 4 times of the simulated ones, suggesting that the (near) resonance enhancement of Raman intensity of *R*-**Ni** is a bit overestimated theoretically.

Overall, the good agreement between simulated and experimental I_R+I_L (Raman) and I_R-I_L (eCP-Raman) spectra in Figure 2 and Figure S3 strongly supports the conclusion that the eCP-Raman mechanism proposed for Equation (1) is the dominant contributor in these systems. The simulated natural RROA spectral patterns of the solutes, on the other hand, look different from the experimental ones. This, together with the strong solvent I_R-I_L bands facilitated only by eCP-Raman, indicates that the natural RROA mechanism plays a negligible role in the experimental I_R-I_L spectra observed in both **Ni** and **Cu** cases.

The third example, *S*-**BN**, is an organic molecule with axial chirality. Using experimental ECD profiles in two different solvents, $CHCl_3$ and CH_3CN, and the experimental concentration information reported in Ref. [12], we performed similar calculations as for **Ni** and **Cu**. The final I_R-I_L simulations of *S*-**BN** in $CHCl_3$ and CH_3CN are summarized in Figure 3, for comparison to the experimental data. In Figure 3, we see a similar situation as for **Ni** and **Cu**. First, the negative I_R-I_L feature of the main *S*-**BN** band observed experimentally is correctly predicted by eCP-Raman. Second, the experimental I_R-I_L spectral features of $CHCl_3$ and CH_3CN are also captured by the simulations, including the positive I_R-I_L band of CH_3CN at 2256 cm^{-1}. Third, the strong

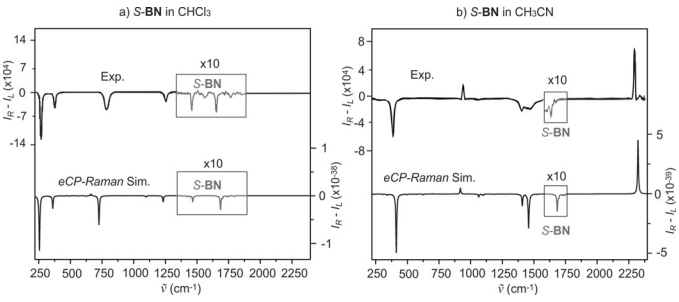

Figure 3. a) Comparison of the experimental[12] (top) and simulated (bottom) I_R-I_L (eCP-Raman) spectra of the chiral solute *S*-**BN** whose bands are shown in the rectangle box and their intensities amplified by a factor of ten, and of achiral solvent $CHCl_3$ whose bands are those outside the box. b) Parallel plots as in (a) but with *S*-**BN** in CH_3CN solution.

experimental I_R-I_L bands of $CHCl_3$ and CH_3CN are about ten times stronger than the main band of *S*-**BN**. This ratio is captured by the simulations. The comparisons shown in Figure 3 clearly demonstrate that one can explain the experimental observation reported in Ref. [12] satisfactorily with the eCP-Raman mechanism, and not by natural RROA.

From Equation (1), one can see that sign of CID depends on the sign of $\Delta\varepsilon$, that is, ECD sign at 532 nm, and that of the term $(\Delta\varepsilon'/\Delta\varepsilon + DOC)$. Since $-1 \le DOC \le 5/7$,[1b] if the $\Delta\varepsilon'/\Delta\varepsilon$ ratio is larger than or near 1, it controls the sign of the $(\Delta\varepsilon'/\Delta\varepsilon + DOC)$ term. This leads to a mono-signate I_R-I_L spectrum, the same sign as that of $\Delta\varepsilon$ at 532 nm, such as in the case of *R*-**Cu**. Appearance of mono-signate I_R-I_L can also result from a more delicate interplay between $\Delta\varepsilon'/\Delta\varepsilon$ versus DOC as in the case of *S*-**BN**. Therefore, for eCP-Raman, single sign I_R-I_L can be observed, as in the case of SES with true molecular RROA.[1,11,24b] However, the mechanisms are different. A mono signate I_R-I_L spectrum does not imply that a SES is in resonance or that the I_R-I_L sign should be opposite to that of ECD.

As shown in Table S1, the CID values of the chiral solutes and of the solvents based on Equation (1) generally agree with the experimental CIDs in the three cases discussed. For example, the experimental CID values are -2.6×10^{-3} for the *R*-**Ni** band at ca. 1588 cm^{-1} and -5.7×10^{-4} for the *R*-**Cu** band at 1520 cm^{-1}, in agreement with the simulated CID values of -4.8×10^{-3} and -8.9×10^{-4}, respectively.

In Figure S4, we compare Raman, CP-Raman and RROA of *R*-**Ni** and *R*-**Cu** calculated at 532 nm with and without the finite-lifetime approach. Clearly, the finite-lifetime approach is crucial for reproducing the experimental I_R-I_L spectrum of *R*-**Ni**. For *R*-**Cu**, on the other hand, the differences are minor. This is consistent with the experimental observation that *R*-**Ni** is the nearest resonance case, then *R*-**Cu**, and finally *S*-**BN**. Not surprisingly, the simulations of *S*-**BN** without the finite-lifetime in Figure 3 already agree well with the experiment.

In all three examples discussed, the eCP-Raman contribution appears to dominate the experimental I_R-I_L observation. Can one detect true RROA of a chiral solute? This may be possible if the CID of true RROA is significantly larger than of eCP-Raman given by Equation (1). Such a condition may be achieved by changing the concentration of the chiral

 © 2021 Wiley-VCH GmbH

solute. Among the three examples, *R*-**Ni** is the most promising one since it is closest to resonance. Nevertheless, several attempts were made to lower *R*-**Ni** concentration to seek RROA without success. In Figure 2, the theoretical RROA intensities predicted at 532 nm are ≈3 times smaller than the simulated I_R-I_L (eCP-Raman) intensities for **Ni**.

On the other hand, RROA intensity depends drastically on the excitation and transition energies, the latter of which are difficult to accurately predict theoretically. Indeed, different levels of theory can give very different RROA. Improvements in instrumentation can be helpful. If the excitation laser wavelength (technically not yet realized at the present time) could be tuned, it may be set to a zero ECD crossing point to mostly avoid ECD interference at the excitation wavelength. However, outgoing Raman scattered light is expected to be still affected by ECD. If a system is very near resonance, the chance to detect true RROA is higher in principle, but this can cause other experimental complications such as stronger absorption and fluorescence.

The current study shows that if there is measurable ECD of a chiral solute at 532 nm at the concentration used for the RROA measurement, the contribution from eCP-Raman cannot be ignored. Strong I_R-I_L achiral solvent bands can be regarded as a hallmark of eCP-Raman, although they may not be visible for weak scatters such as water. It is likely that eCP-Raman contributed in many of the previously reported RROA or even SERROA experimental studies, and their conclusions may need to be re-examined.

Conclusion

We have analyzed I_R-I_L spectra of three typical chiral molecules under (near) resonance in Raman scattering experiments. These resonant I_R-I_L features could be satisfactorily explained by a new form of chiral Raman spectroscopy, eCP-Raman, without detectable contribution from the true, natural RROA. We think that it is of crucial importance to recognize this mechanism when interpreting RROA data, otherwise misleading conclusions about molecular behavior may be drawn. The current study opens the way for a new form of chiral Raman spectroscopy under resonance which is sensitive to natural chirality and structures of chiral molecules. The results also underline the significance of further theoretical development of RROA as a complex and largely unexplored phenomenon.

Acknowledgements

This work was funded by the Natural Sciences and Engineering Research Council of Canada, the Canada Foundation for Innovation, Alberta Enterprise, Advanced Education, the University of Alberta and Compute Canada, and by the Grant Agency (20-10144S) and Ministry of Education (CZ.02.1.01/0.0/0.0/ 16_019/0000729) of the Czech Republic. G.L. acknowledges Alberta Excellence Graduate Scholarship and Gunning Physical Chemistry Fellowship. Y.X. is Tier I Canada Research Chair in Chirality and Chirality Recognition.

Conflict of Interest

The authors declare no conflict of interest.

Keywords: chiral Raman spectroscopy · circularly polarized Raman · electronic circular dichroism · finite-lifetime approach · resonance Raman optical activity

[1] a) L. D. Barron, *Molecular Light Scattering and Optical Activity*, Cambridge University Press, Cambridge, UK, **2004**; b) L. A. Nafie, *Vibrational optical activity: Principles and applications*, Wiley, Chichester, **2011**.
[2] L. D. Barron, *Biomed. Spectrosc. Imaging* **2015**, *4*, 223 – 253.
[3] M. Krupová, J. Kessler, P. Bouř, *ChemPlusChem* **2020**, *85*, 561 – 575.
[4] M. Vargek, T. B. Freedman, E. Lee, L. A. Nafie, *Chem. Phys. Lett.* **1998**, *287*, 359 – 364.
[5] C. Merten, H. Li, L. A. Nafie, *J. Phys. Chem. A* **2012**, *116*, 7329 – 7336.
[6] M. Dudek, E. Machalska, T. Oleszkiewicz, E. Grzebelus, R. Baranski, P. Szcześniak, J. Mlynarski, G. Zajac, A. Kaczor, M. Baranska, *Angew. Chem. Int. Ed.* **2019**, *58*, 8383 – 8388; *Angew. Chem.* **2019**, *131*, 8471 – 8476.
[7] a) S. Haraguchi, M. Hara, T. Shingae, M. Kumauchi, W. D. Hoff, M. Unno, *Angew. Chem. Int. Ed.* **2015**, *54*, 11555 – 11558; *Angew. Chem.* **2015**, *127*, 11717 – 11720; b) R. Sgammato, W. Herrebout, C. Johannessen, *J. Raman Spectrosc.* **2019**, *50*, 1905 – 1913; c) J. Bogaerts, C. Johannessen, *J. Raman Spectrosc.* **2019**, *50*, 641 – 646.
[8] a) S. Abdali, E. W. Blanch, *Chem. Soc. Rev.* **2008**, *37*, 980 – 992; b) S. O. Pour, S. E. J. Bell, E. W. Blanch, *Chem. Commun.* **2011**, *47*, 4754 – 4756; c) S. Ostovar pour, L. Rocks, K. Faulds, D. Graham, V. Parchaňský, P. Bouř, E. W. Blanch, *Nat. Chem.* **2015**, *7*, 591 – 596.
[9] S. Abdali, C. Johannessen, J. Nygaard, T. Nørbygaard, *J. Phys. Condens. Matter* **2007**, *19*, 285205.
[10] J. R. Cheeseman, M. J. Frisch, *J. Chem. Theory Comput.* **2011**, *7*, 3323 – 3334.
[11] L. Nafie, *Chem. Phys.* **1996**, *205*, 309 – 322.
[12] E. Machalska, G. Zajac, M. Baranska, D. Kaczorek, R. Kawęcki, P. F. J. Lipiński, J. E. Rode, J. Dobrowolski, *Chem. Sci.* **2021**, *12*, 911 – 916.
[13] L. N. Vidal, T. Giovannini, C. Cappelli, *J. Phys. Chem. Lett.* **2016**, *7*, 3585 – 3590.
[14] a) S. Luber, J. Neugebauer, M. Reiher, *J. Chem. Phys.* **2010**, *132*, 044113; b) A. Baiardi, J. Bloino, V. Barone, *J. Chem. Theory Comput.* **2018**, *14*, 6370 – 6390; c) J. Mattiat, S. Luber, *J. Chem. Phys.* **2019**, *151*, 234110/1 – 16.
[15] a) S. Luber, M. Reiher, *ChemPhysChem* **2010**, *11*, 1876 – 1887; b) F. Krausbeck, J. Autschbach, M. Reiher, *J. Phys. Chem. A* **2016**, *120*, 9740 – 9748; c) L. Abella, H. D. Ludowieg, J. Autschbach, *Chirality* **2020**, *32*, 741 – 752.
[16] G. L. J. A. Rikken, E. Raupach, *Nature* **1997**, *390*, 493 – 494.
[17] G. Li, J. Kessler, J. Cheramy, T. Wu, M. R. Poopari, P. Bouř, Y. Xu, *Angew. Chem. Int. Ed.* **2019**, *58*, 16495 – 16498; *Angew. Chem.* **2019**, *131*, 16647 – 16650.
[18] T. Wu, G. Li, J. Kapitán, J. Kessler, Y. Xu, P. Bouř, *Angew. Chem. Int. Ed.* **2020**, *59*, 21895 – 21898; *Angew. Chem.* **2020**, *132*, 22079 – 22082. Note a factor of ln 10 was missing in the original derivation.

 © 2021 Wiley-VCH GmbH

[19] a) J. Sadlej, J. C. Dobrowolski, J. E. Rode, *Chem. Soc. Rev.* **2010**, *39*, 1478 – 1488; b) M. Losada, Y. Xu, *Phys. Chem. Chem. Phys.* **2007**, *9*, 3127 – 3135; c) A. S. Perera, J. Thomas, M. R. Poopari, Y. Xu, *Front. Chem.* **2016**, *4*, 9; d) T. Wu, J. Kessler, P. Bouř, *Phys. Chem. Chem. Phys.* **2016**, *18*, 23803 – 23811.
[20] Z. Dezhahang, M. Poopari, J. Cheramy, Y. Xu, *Inorg. Chem.* **2015**, *54*, 4539 – 4549.
[21] R. Clark, S. R. Jeyes, A. J. McCaffery, R. A. Shatwell, *J. Am. Chem. Soc.* **1974**, *96*, 5586 – 5588.
[22] W. Hug, G. Zuber, A. de Meijere, A. F. Khlebnikov, H.-J. Hansen, *Helv. Chim. Acta* **2001**, *84*, 1 – 21.
[23] W. Hug, G. Hangartner, *J. Raman Spectrosc.* **1999**, *30*, 841 – 852.
[24] a) L. Jensen, J. Autschbach, M. Krykunovc, G. C. Schatz, *J. Chem. Phys.* **2007**, *127*, 134101; b) L. A. Nafie, *Theor. Chem. Acc.* **2008**, *119*, 39 – 55; c) T. Helgaker, S. Coriani, P. Jørgensen, K. Kristensen, J. Olsen, K. Ruud, *Chem. Rev.* **2012**, *112*, 543 – 631.
[25] M. J. Frisch, et al., Gaussian development version, Gaussian, Inc., Wallingford, CT, **2020**. See Supporting Information for the full reference.
[26] M. J. Frisch, et al., Gaussian 16, Revision C.01, Gaussian, Inc., Wallingford, CT, **2016**. See Supporting Information for the full reference.

Manuscript received: July 13, 2021
Accepted manuscript online: August 4, 2021
Version of record online: August 27, 2021

 © 2021 Wiley-VCH GmbH